# Variational Models of Pore Networks in Ionomer Membranes: The Role of Electrostatics

K. Promislow[a], J. Jones[a], Z. Xu[b], N. Gavish[a,c], A. Christlieb[a]

[a]Dept. of Mathematics, Michigan State University, East Lansing, MI 48824, USA
[b]Dept. of Mathematical Sciences, Michigan Technological University, Houghton, MI 49931, USA
[c]Dept. of Mathematics, Technion, Haifa, 32000, Isreal

We present a self-consistent, dynamic model for the morphology of the pore networks which form in Nafion and other ionomer membranes when they imbibe solvent. The model incorporates the interactions of the tethered ionic groups with the solvent and the entropic energy of the counter ions. Numerical simulations are presented which display hysteresis, and the development of pearled pore structures. A framework for extensions of the model that couple the electrostatic double layer at the interface of the pore wall and the transport equations for the counter-ions is presented. The framework derives the ionic transport and generalized Poisson equation from an action whose gradient flows dissipate a related free energy, in agreement with the second law of thermodynamics.

## Network Formation in Ionomer Membranes

While ionomer materials play a central role in Polymer Electrolyte Membrane (PEM) fuel cells, may basic questions about the morphology of their pore networks remain unanswered. Nafion is the industry standard for membrane separators in PEM fuel cells due to its high ionic conductivity, mechanical robustness, and durability. It is a peruorosulfonate ionomer membrane with tethered $SO_3H$ acid groups which disassociate in the presence of polar solvent. The chemical energy behind the disassociation leads to one of Nafion's key properties: the imbibition of solvent, principally water, to produce a pore network on the 2-4 nanometer length scale. The network facilitates the conduction of counter-ions, chiefly protons in PEM fuel cell applications, and generates the ionic selectivity of the membrane.

There have been many proposed forms for the ionic-cluster morphology, i.e., the solvent-filled pore network, of Nafion. Early SAXS experiments, (1)-(2), lead Hsu and Gierke to hypothesize that a balance between the elastic energy of the interface and the hydrophilic surface interactions among the charged functional groups and the solvent drive Nafion to generate a water-filled, "pearled" pore network comprised of small 4-5 nanometer balls interconnected by thin 1-2 nanometer cylindrical pores, see Figure 4 (bottom-right). Nanoscale pearling has also be studied in functionalized diblock polymers, (3)-(4). The morphologies of Hsu and Gierke are somewhat controversial, as numerical and experimental investigation of the microstructure of Nafion and related perfluorinated membanes

have lead to the proposition of bi-layer morphologies, (5)-(6), cylindrical pores, (7), an inverted pore morphology with solvent groups surrounding cylinders of crystallized backbone, (8)-(9), spherical clusters, (10). However, even at a course-grained level, molecular and dissipative particle dynamics simulations of solvated, hydrophilic-hydrophobic polymer systems cannot compute the morphological development to its equilibrium, (11)-(15) even in state-of-the-art simulations resolved to milliseconds of real time, (16). Indeed Magnetic Resonance Imaging experiments evidence suggests that the pore network within PFSAs undergoes 10-20 hour transients after changes in external environment, (17). Continuum models of network formation in Nafion, (18)-(20), have successfully predicted geometric features, such as pore radius and overall solvent uptake as a function of ionic group density, liquid phase pressure, and effective elastic response of the polymer phase. Central to each of these models is the assumption that the ionic groups aggregate in the perfluorinated polymer matrix to form a connected network of clusters that allow for significant swelling by polar solvents and efficient proton transport through the corresponding nanometer-scale domains. However these models do not predict the morphology from a thermodynamic formulation, nor can they suggest possible modes of evolution of the network, since the network morphology is taken as a model assumption.

## The Functionalized Cahn-Hilliard Interfacial Free Energy

The Functionalized Cahn-Hilliard (FCH) free energy, presented in (21), incorporates the effects of solvation energy, counter ion entropy, and elastic backbone stiffness into a thermodynamically self-consistent formulation for the resultant polymer-solvent morphology. Indeed, the over-damped (gradient) flows of the FCH free energy recover many of the proposed morphological complexities of polymeric membranes. The underlying idea is to search for the solvent network phase among the *critical points* of the Cahn-Hilliard free energy – as distinct from the minimizers. It is well understood that minimizers of the Cahn-Hilliard energy correspond to morphologies which minimize the surface area of the interface. However the introduction of the tethered, charged groups within the ionomer membrane, the $SO_3^-$ groups in Nafion, dramatically alters the energy landscape. The solvent phase can greatly lower the electrostatic energy of the mixture by screening the charge, which rewards the generation of interface. Moreover the counter-ions, which for Nafion are comprised of protons in the form of excess hydrogen bounds, reside in the solvent phase where they experience a mixture of strong effects, from the electrostatics which pull them towards the negative charges to interactions with the dipole field of the polar solvent, whose dielectric field they strongly impact.

The Cahn-Hilliard energy for the solvent volume fraction $u$ which is 0 in a polymer phase and 1 in the pure solvent phase takes the form

$$\mathcal{E}(u) = \int_\Omega \frac{\epsilon^2}{2}|\nabla u|^2 + W(u;\tau)\,dx \qquad [1]$$

where the double well function $W$ has two local minima, one at $u = 0$ and a second at $u = 1$. Significantly, the value of $W$ at the two minima, the self-energy of the pure

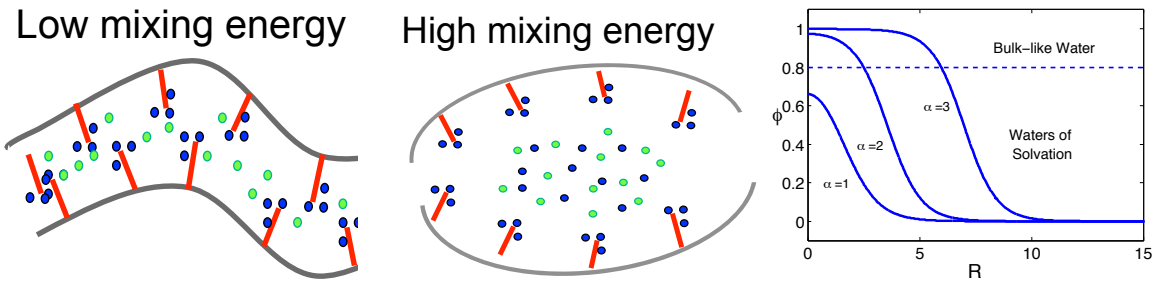


Figure 1: (Left) Interaction of solvent with tethered and free counter-ionic groups for different values of mixing energy $\eta_m$. The value of $\eta_m$ reflects the entropic penalty for high densities of interspersed ions and counter ions. Larger values of $\eta_m$ lead to segregation of charge groups on the length scale of the pore. (Right) Cross-section profiles of bilayer (co-dimension $\alpha = 1$), pore ($\alpha = 2$), and micelle ($\alpha = 3$) profiles showing that the higher co-dimensional structures correspond to larger reservoir of "pure" solvent phase, which leads to a higher value of the dielectric constant in the bulk-like solvent.

states, need not be equal. The double well can be constructed from an equal-depth well $W_0(u) = \frac{1}{2}u^2(u-1)^2$, via the tilt parameter $\tau > 0$,

$$W(u;\tau) := W_0 - \tau \int_0^u \sqrt{W_0(s)}ds, \qquad [2]$$

so that $W$ satisfies $W'(0) = W'(1) = 0$ while $W(0) = 0 > W(1)$. The well-tilt controls the relative values of the self-energy of the two phases. The parameter $\epsilon > 0$ is the dimensionless ratio of the domain size to the width of the interfaces separating the distinct phases. The critical points of the Cahn-Hilliard are the zeros of the variational derivative,

$$\frac{\delta \mathcal{E}}{\delta u}(u) := -\epsilon^2 \Delta u + W'(u;\tau) = 0. \qquad [3]$$

These critical points include not only the familiar minimal surfaces, but also the large families of network structures. Indeed the principal ingredients of the network morphologies are the symmetric solutions $\phi$ of

$$\partial_R^2 \phi + \frac{\alpha - 1}{R}\partial_R \phi = W'(\phi), \qquad [4]$$

corresponding to the critical point equation with co-dimension $\alpha = 1, 2$, or 3, which are the bi-layer, pore, and micelle profiles depicted in Figure 1. The process of *functionalization* stabilizes these structures, replacing the Cahn-Hilliard energy with the square of its variational derivative. *Every* critical point of the Cahn-Hilliard energy is a global minimizer of its primative functionalized form

$$\mathcal{F}_0(u) := \int_\Omega \frac{1}{2}\left(\frac{\delta \mathcal{E}}{\delta u}\right)^2 dx = \int_\Omega \frac{1}{2}\left(\epsilon^2 \Delta u - W'(u;\tau)\right)^2 dx. \qquad [5]$$

The energy $\mathcal{F}_0$ is very degenerate – to stimulate the growth and control the morphology of network structures, small terms are subtracted which reward the generation of surface area and incorporate counter-ion entropy. The result is the Functionalized Cahn-Hilliard free energy

$$\mathcal{F}(u) := \int_\Omega \frac{E_b}{2}\left(\epsilon^2\Delta u - W'(u;\tau)\right)^2 - \eta_h\frac{\epsilon^2}{2}|\nabla u|^2 - \eta_m W_m(u)\,dx. \qquad [6]$$

The dominant term, $\mathcal{F}_0$ multiplied by a backbone stiffness parameter $E_b$, is minimized precisely when the phase variable $u$ is a critical point of the Cahn-Hilliard energy. The critical points can be either bilayer, pore, or micellular network structures, whose diameter is scaled by $\epsilon$ but also parameterized by the well tilt parameter $\tau$, see Figure 1 (right). The free energy $\mathcal{F}_0$ is perturbed by two small, *negative* terms parameterized by $0 < \eta_h, \eta_m \ll E_b$. The $\eta_h$ perturbation represents the energy *liberated* per unit area of interface formed, and relates to the density and hydration energy of the tethered ionic groups. The second parameter denotes the relative tolerance of the counter-ions for low verses high dielectric solvent. Unlike the tethered ionic groups, the counter ions are free to reorganize. The parameter $\eta_m$ characterizes the entropy of mixtures of ions, counter-ions, and solvent. At a formal level, this can be though of as a finite volume exclusion for the charged groups, which is anomalously high for protons, see Figure 1 (left).

As a first step, we consider the evolution of morphologies via a gradient flow of the FCH energy over a periodic domain $\Omega \subset \mathbf{R}^3$,

$$u_t = \Delta\frac{\delta\mathcal{F}}{\delta u} = \Delta\Big[E_b\left(\epsilon^2\Delta - W''(u)\right)\left(\epsilon^2\Delta u - W'(u)\right) + \eta_h\epsilon^2\Delta u - \eta_m W_m'(u)\Big]. \qquad [7]$$

As presented in (21), this flow leads to a decrease of the free energy,

$$\frac{d}{dt}\mathcal{F}(u) = -\int_\Omega \left|\nabla\frac{\delta\mathcal{F}}{\delta u}\right|^2 dx \le 0. \qquad [8]$$

For non-zero values of the well tilt parameter, $\tau > 0$, the mixing energy parameter $\eta_m$ has a strong impact on the morphology of the solvent network as it evolves, driving the morphology towards bilayer, pore, pore-micelle, or pure micelle structures depending upon the values of $\eta_m$, see Figure 2. The pore structure of Nafion relaxes on time-scales of tens of hours, (17), and is well-known to be hysteric. This hysteresis is also present in the FCH model. Taking random initial data with a solvent volume fraction of 30%, consistent with Nafion boiled in acid, and then slowly evaporating solvent down to 8% volume fraction, slow here is in comparison to evolution timescales of the morphology, leads to a sparse pore network. Conversely, a direct relaxation of random initial data with an 8% solvent volume fraction would lead to a disjoint, that is a non-percolating, pore network. This simulation suggests that the standard processing to transition Nafion from its shrunk form to yield the normal form by passing through the expanded form produces spatially distributed pore networks which percolate at minimal water content.

In (1), Hsu and Gierke proposed a pearled-pore structure of the solvent phase, based upon a balance between elastic energy of the backbone and hydration energy of the tethered groups. This balance finds analogy within the FCH energy, particularly between the

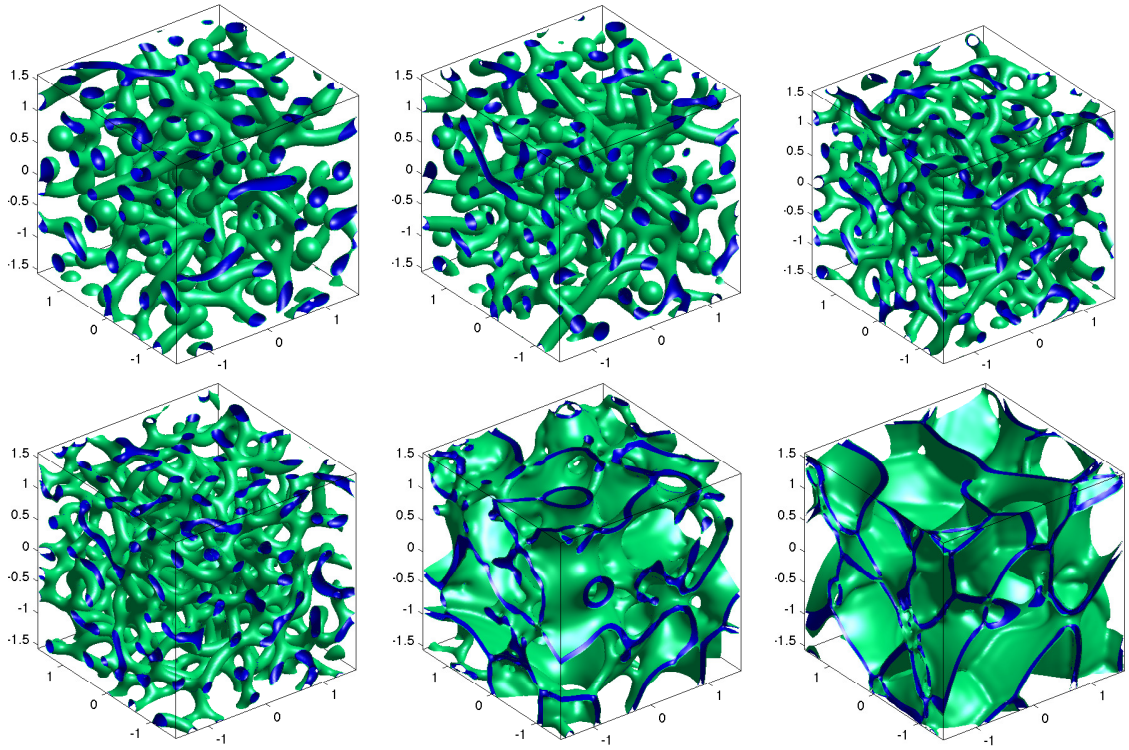

Figure 2: Network structures from *identical* initial data of 20% solvent volume fraction. The image is of two level sets of $u$, a lower one colored green and a higher (solvent phase) colored blue. In all simulations $E_b = 1$, $\epsilon = 0.03$, $\tau = 0.4$ and $\eta_h = 0.15$, while the counter-ion entropy takes the values $\eta_m = -0.06, -0.03, 0, 0.06, 0.15, 0.27$, from left to right and top to bottom. A large value of $\eta_m$ leads to a preference for lower co-dimensional structures

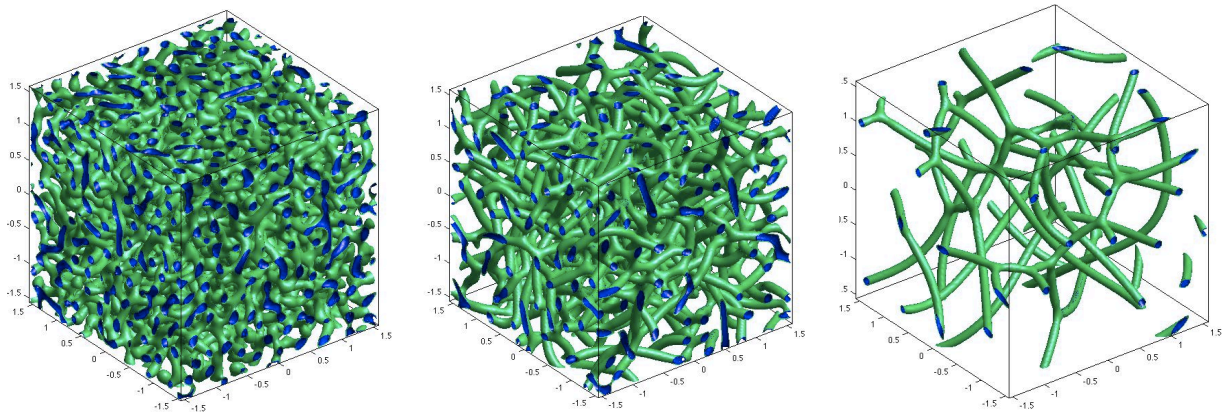

Figure 3: Pore network evolution under evaporation of solvent phase. Starting from random initial data, the solvent phase is slowly reduced from 30.2% to 19.7% to 8.24% solvent volume fraction (left to right). The final state is unattainable from random initial data with the same volume fraction; the hysteresis loop of over-hydration and evaporation emulates the boiling of dry Nafion in acid and the subsequent desiccation treatment which is typical to render Nafion to its "normal" form. Parameters are $\tau = 0.4$, $\epsilon = 0.03$, $\eta_h = 0.03$ and $\eta_m = 0.12$.

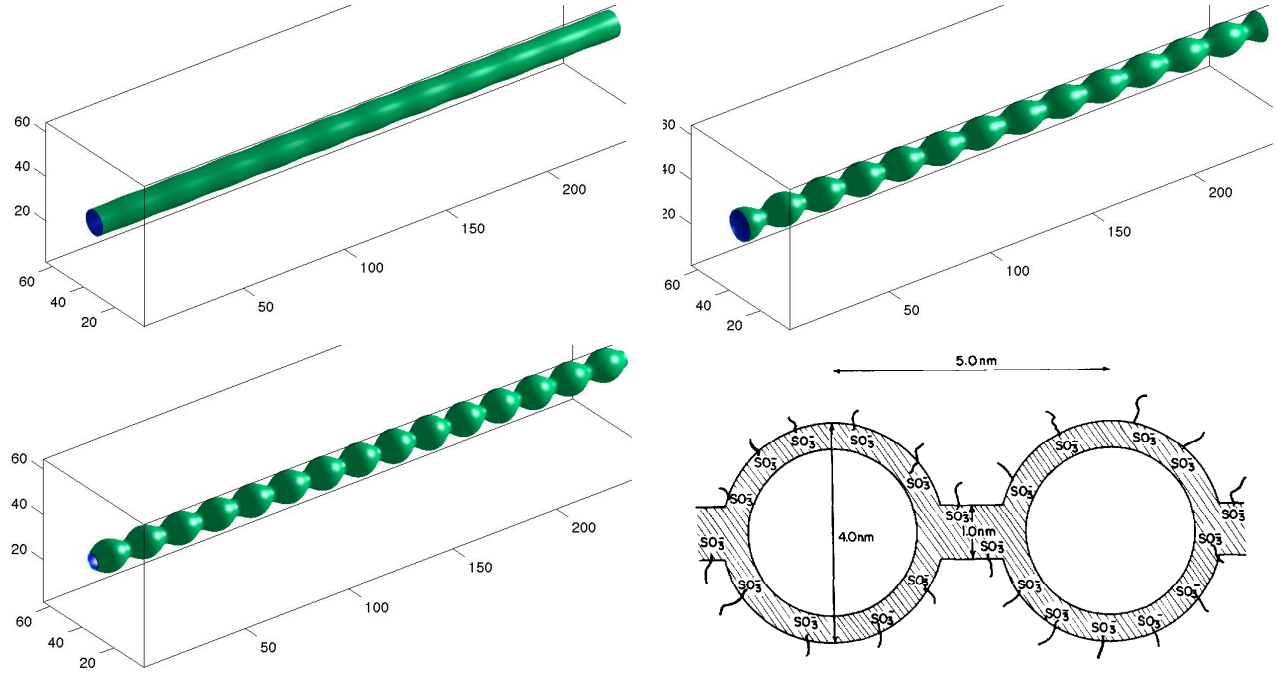


Figure 4: Pearled equilibria obtained by evolution from a cylindrically symmetric, radially perturbed pore for $\epsilon = 0.03$, $\eta_h = 0.03$ and $\eta_m = 0.12, 0.24, 0.3$, respectively left to right. (Bottom-right) Cartoon of the pearled-pore ionic cluster morphology of Nafion proposed in (1) based upon a balance of elastic deformation and hydrophilic energies.

$E_b$ and $\eta_h$ terms. As was shown in (21), the residual of the $\mathcal{F}_0$ term is the square of the mean curvature of the interface, which is analogous to the elastic energy of the deformation of the interface. However it is the counter-ion mixing energy which controls the bifurcation of the pearled-pore structures within the FCH energy. As shown in Figure 4, for $\epsilon = 0.03$, $E_b = 1$, $\tau = 0.4$ and $\eta_h = 0.03$, a cylindrically symmetric pore is stable to perturbations if $\eta_m = 0.12$, but at higher values it relaxes into a pearled structure with the radii of the pearled phase increasing with the mixing energy coefficient, $\eta_m$. In Figure 5, the water content of a straight, cylindrical pore is increased from 8.11% to 9.50% of the total volume of the bounding domain. However the value of the well-tilt parameter, $\tau$, fixes the equilibrium radius of the cylindrical pore, so that additional water must be accommodated through a micelle structure, which has a greater radius than the pore – see Figure 1 (right). The cylindrical pore passes through a continuum of pearled states to arrive at a disjoint collection of micelles as it swells to accommodate the additional water volume fraction. We were unable to induce the pearling bifurcation in the random pore networks presented in Figure 3. A possible explanation is that the random networks are free to adjust their length to accommodate an optimal amount of solvent phase per unit length. In a physical sample of Nafion the tethered charges are less free to reconfigure due to elastic energy. This constraint could serve to induce the pearling bifurcation as solvent loading is varied. This and other extensions of the model are considered in the next section.

## Extensions of the Model

The FCH is merely a description of the free energy landscape associated to the solvent-polymer interface, an accurate description of Nafion and other ionomer materials must encompass more than a binary mixture of charged polymer and solvent. Extensions of the model should include:

- A continuum resolution of the pressure and elastic forces. The local pressure in the liquid phase is an intrinsic component of the self-energy of the liquid and should couple to the value of he well tilt parameter $\tau$. That is, the pores should expand ($\tau$ larger) or contract ($\tau$ small) as the pressure in the liquid phase increases or decreases.
- A mechanism to track the local density of tethered ionic groups as the pores swell and shrink. This can be achieved by coupling the value of $\eta_h$ to the local average water content.
- A description of the counter-ion distribution, their coupling to the interface energy, and to the transport of solvent within the pore network.

The remainder of this paper addresses a self-consistent extension which incorporates a dynamic transport model for the counter-ions within the pore network; providing a framework in which the $\eta_h$ and $\eta_m$ parameters can be related to more classically defined electrostatic quantities. We do not address the coupling between the counter-ions and the fluid phase, nor the elastic energy which links the polymer phase to the crystalline network.

### Electrostatics and Ion Transport

Many models in the literature couple Poisson's equation to ionic transport to produce a flow which dissipates a free energy, see (22) for a review of this field. Some are based upon a dielectric which varies with electric field intensity, as proposed by Booth (23), and adapted to fuel cell applications by Bontha and Pintauro (24), with subsequent corrections by Paul and Paddison (25) and (26). However, in fuel cell applications the Stern layer, in which finite size effects are significant, is a non-trivial percentage of the total pore radius. In particular, resolving distributions in which positive and negative ions are physically separated, despite their electrostatic attraction, requires the inclusion of the solvent phase in a nontrivial manner. Moreover, incorporating the solvent phase via a dependence of the effective dielectric upon the electric field strength is not sufficient, as this can lead to unphysical crowding of charges. Indeed, in continuum models, an electro-neutral solution of ionic groups of *arbitrary* density produces no electric field. In models such as Booth's, high densities of neutral ions would produce no net electric field and the dilectric of the solvent would be that of the bulk phase. When addressing length scales below 1 nanometer, it is physically reasonable to account not only for the total charge imbalance, but also the total charge density. This can be achieved through finite-volume effects, see for example (27), or through an explicit dependence of the dielectric upon the total charge density (28).

The framework presented below incorporates each of these effects, and couples them

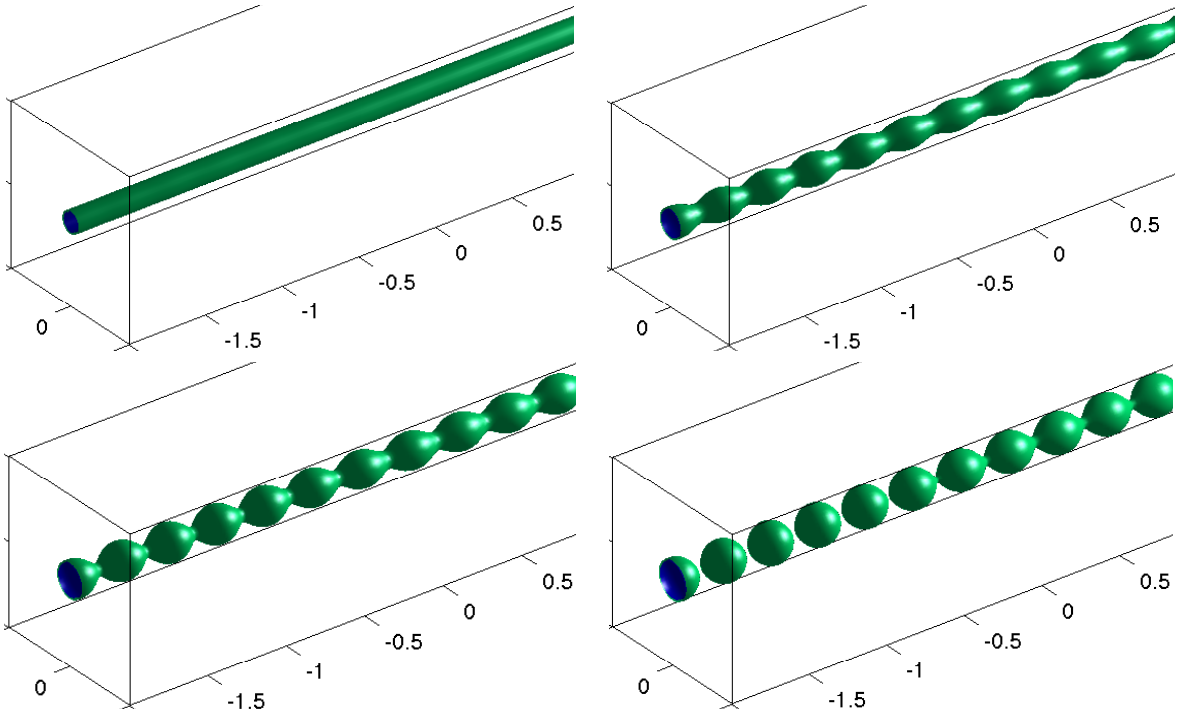


Figure 5: Pearled equilibria obtained as the water content of the pore is increased through 8.11%, 8.69%, 9.22%, to 9.50% (left to right and top to bottom) of the total mass of the bounding box. The parameters are $\epsilon = 0.03$, $\eta_h = 0.15$, $\eta_m = 0.24$.

to the primitive interfacial free energy, $\mathcal{F}_0$, in such a way that the combined evolution dissipates the total free energy. The solvent phase of Nafion contains a single, monovalent positive and negative ionic species, with the density of the positive ions, denoted by $p$, transported within the fluid phase, and while the negative ionic density, $n = n(u)$, is slaved to the phase-field variable $u$. The negative charges have a slowly varying and rapidly varying component

$$n(u) = n_{\max} \overbrace{(1 - G * u)}^{\text{slow}} \overbrace{W_0(u)}^{\text{rapid}}. \qquad [9]$$

The value $n_{\max}$ is a maximal reference density of acid groups, achieved at the dry state. The rapidly varying component is parameterized by $W_0$, the symmetric double well which is zero at both the pure polymer phase, $u = 0$, and the pure solvent phase, $u = 1$. This results in a ion density that is localized on the polymer-solvent interface where $0 < u < 1$. The slowly varying component models the dilution of ionic groups with the swelling of membrane, and serves to keep the total density of ionic groups proportional to the total density of the polymeric phase as the membrane swells and contracts. This is account for through the convolution,

$$(G * u)(x) = \int_\Omega G(x - y)u(y)\, dy, \qquad [10]$$

with a normalized Gaussian weight, $G(z) = \exp(-|z|^2/L^2)/(\pi^{3/2}L^3)$, with characteristic length scale $L \gg \epsilon$. The electric field is expressed as the gradient of its potential, $E = \nabla\phi$, and the dielectric may depend upon the electric field not only through the square intensity of the electric field, $I = |\nabla\phi|^2$, but also through the density of the charge groups.

In statistical mechanics it is standard to obtain a continuum description from the mean-field approximation of the partition function. The approach presented here is a computationally simpler methodology to derive a coupled flow which dissipates a total free energy. It begins with an action of the general form

$$\mathcal{A}(\phi, p, n, u) = \int_\Omega \overbrace{k_B T\Big(p\ln p + h(p, n(u))\Big)}^{\text{finite volume}} + \overbrace{q_0(p-n)\phi - \frac{1}{2}\overline{\varepsilon}(I, p, n)}^{\text{electrostatic}}\, dx, \qquad [11]$$

where $h$ denotes the form of the short-range or finite-volume energy, $q_0$ is the elemental charge, and $\overline{\varepsilon}$ is related to the polarization or displacement field induced by the electric field, as is expanded upon below. The charge densities $p$ and $n$ have been non-dimensionalized by the factor of $10^{-8}\mathrm{C/m}^3$. The electric field is required to be a critical point of the action, yielding a generalized Poisson equation,

$$\frac{\delta\mathcal{A}}{\delta\phi} := \nabla\cdot\left(\frac{\partial\overline{\varepsilon}}{\partial I}\nabla\phi\right) + q_0(p-n) = 0, \qquad [12]$$

in particular the classic orientational permittivity (dielectric) takes the form

$$\varepsilon := \frac{\partial\overline{\varepsilon}}{\partial I} = -2\frac{\delta\mathcal{A}}{\delta I}. \qquad [13]$$

Up to a rescaling, this formulation of the dielectric is equivalent the standard derivation of statistical mechanics, see (26) (equations (6), (10), and (11)) for example. Substituting for the charge density, $p-n$, from Poisson's equation in $\mathcal{A}$, and integrating by parts with the periodic boundary conditions yields an energy,

$$\mathcal{E}_\mathcal{A}(\phi, p, n) = \int_\Omega \left(k_B T(p\ln p + h(p,n)) + I\frac{\partial\overline{\varepsilon}}{\partial I} - \frac{1}{2}\overline{\varepsilon}\right) dx, \qquad [14]$$

which is bounded below if $\overline{\varepsilon}$ is convex in $I$. Taking the evolution of the protonic groups as a gradient flow on the action yields a Nernst-Planck type equation

$$\begin{aligned} p_t &= \tfrac{D_p}{k_B T}\nabla\cdot\left(p\nabla\tfrac{\delta\mathcal{A}}{\delta p}\right), \\ &= D_p\nabla\cdot\left(\left[1 + p\tfrac{\partial^2 h}{\partial p^2}\right]\nabla p + p\tfrac{\partial^2 h}{\partial p\partial n}\nabla n + \tfrac{p}{k_B T}\nabla\left(\phi - \tfrac{1}{2}\tfrac{\partial\overline{\varepsilon}}{\partial p}\right)\right). \end{aligned} \qquad [15]$$

The combined Poisson-Nernst-Planck system, [12]-[15], satisfies the second law of Thermodynamics, via the Onsager relation,

$$\frac{d\mathcal{E}_\mathcal{A}}{dt} = -\frac{D_p}{k_B T}\int_\Omega \left|\nabla\frac{\delta\mathcal{A}}{\delta p}\right|^2 dx \le 0, \qquad [16]$$

with the dissipation mechanism attributed to the charged particle motion.

Development of the Action. The electrostatic energy is better understood than the action. This requires an inversion of the procedure outlined above, using the energy to derive the action and then the Poisson and Nernst-Plank equations. The energy density of an electric field $E$ with displacement field $D$ takes the form

$$\mathcal{E}_{\text{elect}} := \int_\Omega \frac{1}{2} E \cdot D \, dx. \tag{17}$$

As is consistent with the framework, the displacement field is taken in the form

$$D = \varepsilon_r(p,n)E + \overline{D}(I,n,p)E,$$

where $\varepsilon_r$ is a reference dielectric for water and the term $\overline{D}$ incorporates higher order effects of the electric field upon the displacement field. Incorporating the short-range, finite volume effects, the combined short range-long range free energy takes the form

$$\mathcal{E}_{\text{SL}}(\phi,p,n) = \int_\Omega \overbrace{k_B T\Big(p\ln p + h(p,n)\Big)}^{\text{finite volume}} + \overbrace{\frac{1}{2}\left(\varepsilon_r(p,n) + \overline{D}(I,p,n)\right) I}^{\text{electrostatic}} \, dx. \tag{18}$$

The requirement that the action $\mathcal{A}$, generate the short range-long range energy, that is $\mathcal{E}_{\mathcal{A}} = \mathcal{E}_{\text{SL}}$. Equating [18] and [14] requires linking $\overline{\varepsilon}$ to $\overline{D}$ via the differential equation,

$$I\frac{\partial \overline{\varepsilon}}{\partial I} - \frac{1}{2}\overline{\varepsilon} = \frac{1}{2}\varepsilon_r(p,n) + \overline{D}(I,p,n), \tag{19}$$

which is well-posed if supplemented with the zero intensity ($I = 0$) initial condition

$$\overline{\varepsilon}(0,p,n) = -\varepsilon_r(p,n) - 2\overline{D}(0,p,n). \tag{20}$$

The corresponding action is denote $\mathcal{A}_{\text{SL}}$.

Fully Coupled Model. Combining the electrostatic energy with the interfacial energy produces a combined free energy,

$$\mathcal{T}(u,p,\phi) := E_b\mathcal{F}_0(u) + \mathcal{E}_{\text{SL}}(u,p,\phi), \tag{21}$$

where the dependence of $\mathcal{E}_{\text{SL}}$ on $u$ is through $n = n(u)$. The associated action is

$$\mathcal{A}_{\mathcal{T}} = E_b\mathcal{F}_0(u) + \mathcal{A}_{\text{SL}}(u,p,\phi). \tag{22}$$

The gradient flow of the action,

$$u_t = \Delta\frac{\delta \mathcal{A}_{\text{T}}}{\delta u} = \Delta\left[E_b\frac{\delta \mathcal{F}_0}{\delta u} + \left(k_B T\frac{\partial h}{\partial n} - q_0\phi - \frac{1}{2}\frac{\partial \overline{\varepsilon}}{\partial n}\right)\frac{\partial n}{\partial u}(u)\right], \tag{23}$$

$$p_t = \frac{D_p}{k_B T}\nabla\cdot\left(p\nabla\frac{\delta \mathcal{A}_{\text{T}}}{\delta p}\right) = \frac{D_p}{k_B T}\nabla\cdot\left[p\nabla\frac{\delta \mathcal{A}_{\text{SL}}}{\delta p}(u,p,\phi)\right], \tag{24}$$

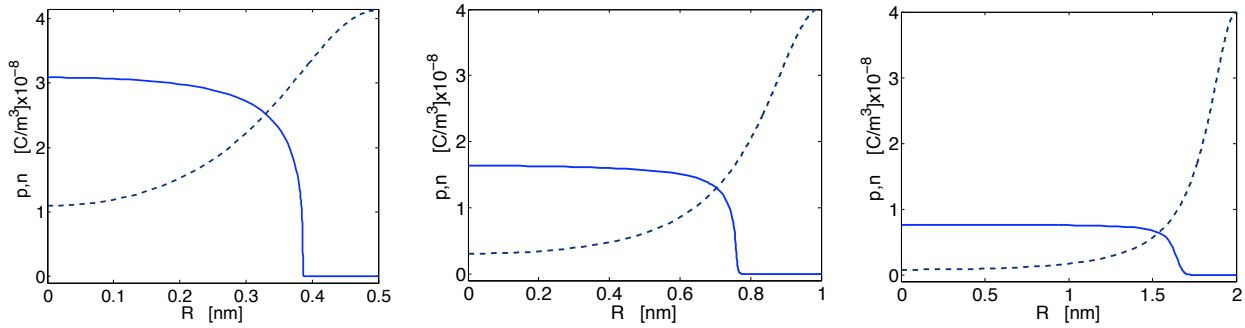


Figure 6: Distribution of positive (blue-solid) and negative (red-dashed) ions between two plates as a function of the distance $R$ from center-line. From the plate half-width is $0.5, 1.0$, and $2.0$ nanometers, and the prescribed negative ion profile corresponds to $0.3-0.4$ C/m$^2$ of surface charge. The positive ion profile is computed from the steady-state system [30]-[31].

couples with Poisson's equation, [12] to dissipate the total free energy $\mathcal{T}$,

$$\frac{d}{dt}\mathcal{T}(u,p,\phi) = -\int_\Omega E_b \left|\nabla \frac{\delta \mathcal{F}_0}{\delta u}\right|^2 + \frac{D_p}{k_B T} p \left|\nabla \frac{\delta \mathcal{A}_{\rm SL}}{\delta p}\right|^2 dx \le 0, \qquad [25]$$

via the motion of the positive charge density $p$ and the phase field $u$. While [24] differs from [15] only in the particular choice of $\overline{\varepsilon}$, it is intriguing to compare the phase separation equation [23] with the FCH gradient flow [7]. Indeed the perturbation terms are now derived directly from the short range-long range action, $\mathcal{A}_{\rm SL}$. The addition terms on the right-hand side of [23] couple the capacitance $\overline{\varepsilon}$, electrostatic field $\phi$, and counter-ion entropy $h$ directly to the phase separation. It is tempting to make the associations

$$\eta_h \frac{\epsilon^2}{2}|\nabla u| \approx \left(q_0\phi + \frac{1}{2}\frac{\partial \overline{\varepsilon}}{\partial n}\right)\frac{\partial n}{\partial u}, \qquad [26]$$

$$\eta_m W_s(U) \approx -k_B T \frac{\partial h}{\partial n}\frac{\partial n}{\partial u}. \qquad [27]$$

A careful study of the two models to better understand the functional dependence of the hydration and mixing energies within the FCH is a particularly rich vein for future investigation. In the remaining section we investigate the impact of the electrostatic portion of the model on the charge distribution within a simple channel.

## Charge Distribution with a Channel

The short range-long range formulation of the electrostatic energy encompasses many prior models of the energy of a mixture of monovalent ions and solvent. Dropping the influence of the phase field, $u$, the physical domain is fixed as a simple channel, and the negative charges given a prescribed spatial variation $n = n(x)$, see Figure 6. The classic Poisson-Nernst-Planck system, also known as the Gouy-Chapman model, is recovered by setting

$$\overline{D} \equiv 0, \quad \varepsilon_r = \epsilon_0, \quad h \equiv 0,$$

so that the primitive of the dielectric takes the form $\bar{\varepsilon} = -\varepsilon_0$, with $\varepsilon_0$ a reference bulk value for water. The finite-volume terms are modified from those of Di-Caprio et al. (27), taking the form

$$h(p,n) = p\left(\frac{p^2}{p_c^2} + \frac{n^2}{n_c^2}\right), \qquad [28]$$

where the critical values of positive and negative ion densities are $p_c = 1.4$ and $n_c = 1$ in the dimensionless units. The pore geometry $u$ is frozen as a planar bilayer of half-width $R$, and the coupled evolution is taken at equilibrium, for which [12] and [15] reduce to the Nernst-Planck system

$$\nabla \cdot \left((1 + \frac{6p^2}{p_c^2})\nabla p + \frac{2pn}{n_c^2}\nabla n + \frac{pq_0}{k_B T}\nabla\phi\right) = 0, \qquad [29]$$

coupled to Poisson's equation

$$\nabla \cdot (\epsilon_0 \nabla\phi) = n - p. \qquad [30]$$

At equilibrium the flux of protonic charge is zero, and the Nernst-Planck equation reduces to an algebraic system,

$$\ln p + \frac{3p^2}{p_c^2} + \frac{n^2}{n_c^2} + \frac{q_0\phi}{k_B T} = C, \qquad [31]$$

where the constant $C$ is determined to enforce global electroneutrality across the channel. The combined system, [30] and [31] is solved subject to the global electroneutrality condition, $\phi' = 0$ on the walls of the channel. As depicted in Figure 6, for different channel widths with the same prescribed total charge, approximately 0.4 C/m$^2$ of surface area, the positive charges are driven away from the regions of maximal negative charge, which leads to a strong local charge imbalance, while maintaining global charge neutrality.

**Acknowledgements**

The first author acknowledges support from the National Science Foundation through grants DMS 0708804, DMS 0934568, and DMS 1125231.

# References

1. W. Hsu and T. Gierke, *J. Membrane Science* **13**, 307(1983).
2. S. Kumar and M. Pineri, *J. of Polymer Sci. Part B - Polymer Physics* **24**, 1767(1986).
3. G.M. Grason and C. D. Santangelo, *European Phys. J. E* **20** 335 (2006).
4. F. Campelo and A. Hernández-Machado, *PRL* **99** 088101 (2007).
5. H. W. Starkweather,*Macromolecules* **15**, 320 (1982)
6. A. V. Krivandin, A.B. Solov'ena, N. N. Glagolev O.V. Shatalova, S. L. Kotova, *Polymer* **44**, 5789 (2003).
7. K. Schmidt-Rohr and Q. Chen, *Nature Materials* **7**, 75 (2008)
8. L. Rubatat, A. L. Rollet, G. Gebel, and O. Diat, *Macromolecules* **35**, 4050 (2002)
9. L. Rubatat, G. Gebel, and O. Diat, *Macromolecules* **37**, 7772 (2004)
10. J. A. Elliott, S. Hanna, A. M.S. Elliott, and G. E. Cooley, *Macromolecules* **33**, 4161(2000).
11. D.S. Wu, S. J. Paddison, and J. A. Elliott, *Energy and Environmental Sci.* **1**, 284 (2008)

12. D. S. Wu, S.J. Paddison, and J. A. Elliott, *Macromolecules* **42**, 3358 (2009)
13. K. D. Kreuer, S. J. Paddison, E. Spohr, E and M. Schuster, *Chem. Rev.* **104**, 4637 (2004)
14. S.J. Paddison, and K. S. Promislow, eds., *Device and Materials Modeling of Polymer Electrolyte Membrane Fuel Cells*, Springer, New York (2009).
15. C. Knox and G. A. Voth, *J. Phys. Chem. B* **144**, 3205 (2010).
16. B. G. Levine, D. N. LeBard, R. DeVane, W. Shinoda, A. Kohlmeyer, and M. L. Klein, *J. of Chem. Theory and Comp.* **7**, 4135 (2011).
17. Z. Zhang, K. Promislow, J. Martin, H. Wang, B. Balcom, *J. Power Sources* **196** 8525 (2011).
18. A. Z. Weber and J. Newman, *Chem.l Rev.* **104** 4679 (2004).
19. A. Z. Weber and J. Newman, *J. Electrochem. Soc.* **151** A311(2004).
20. E. Eikerling and P. Berg, *Soft Matter* **7**, 5976 (2011).
21. N. Gavish, J. Jones, Z. Xu, A. Christlieb, K. Promislow, *Polymers* **4** 630 (2012).
22. M. Bazant, M. Kilic, B. Storey, and A. Ajdari, *Adv. Colloid Interface Sci.* **106** 104119 (2009).
23. F. Booth, *J. Chem. Phys.* **19**, 391 (1950).
24. J. R. Bontha and P. N. Pintauro, *Chemical Engineering Science* **49** 3835 (1994).
25. R. Paul and S. J. Paddison, *J. Chem. Phys.* **115**, 7762 (2001).
26. R. Paul and S. J. Paddison, *J. Phys. Chem. B* **108** 13231(2004).
27. D. di Caprio, Z. Borkowska, and J. Stafiej, *J. Electroanal. Chem.* **572** 51(2004).
28. M. Hatlo, R. van Roij, and L. Lue, *Europhysics Letters* **97** 28010 (2012).